Journal of Colloid and Interface Science 343 (2010) 65–70

Contents lists available at ScienceDirect

Journal of Colloid and Interface Science

www.elsevier.com/locate/jcis

Control of the morphology and size of magnetite particles with peptides mimicking the Mms6 protein from magnetotactic bacteria

Atsushi Arakaki, Fukashi Masuda, Yosuke Amemiya, Tsuyoshi Tanaka, Tadashi Matsunaga *

Department of Biotechnology, Tokyo University of Agriculture and Technology, 2-24-16 Naka-cho Koganei, Tokyo 184-8588, Japan

ARTICLE INFO

Article history:
Received 11 September 2009
Accepted 19 November 2009
Available online 26 November 2009

Keywords:
Biomineralisation
Biomimetic material
Peptide
Nanoparticle
Magnetotactic bacteria
Magnetic particles

ABSTRACT

Mms6 is a dominant protein that tightly associates with the surface of bacterial magnetites in *Magnetospirillum magneticum* AMB-1. The protein has previously been shown to mediate the formation of uniform magnetite crystals of cubo-octahedral morphology consisting of (1 1 1) and (1 0 0) crystal faces with a narrow size distribution during chemical magnetite synthesis. In order to understand the role of this protein in chemical magnetite synthesis, magnetite formation was investigated using synthetic peptides mimicking the Mms6 protein. Particles that were synthesized in the presence of short peptides harbouring the C-terminal acidic region of Mms6 exhibited a spherical morphology with circularities of 0.70–0.90 similar to those of bacterial magnetites and particles formed in the presence of the Mms6 protein. In contrast, a rectangular morphology with circularities of 0.60–0.85 were obtained when other peptides were used for synthesis. The results indicated that the C-terminal region of the Mms6 protein has significant control over the morphology of magnetite crystals in the chemical synthetic method. This method can, therefore, be useful as an alternative method of controlling the size and morphology of magnetite crystals under ambient conditions.

1. Introduction

Organisms produce complex nanostructures consisting of inorganic and organic components that form a variety of self-organized and hierarchical structures [1,2]. These highly organized structures often exhibit excellent physical and/or chemical properties that are superior to those of artificial materials [3]. Furthermore, the intricate architecture of biominerals is formed under fairly mild conditions compared to those in the case of the usual synthetic methods. Recent molecular studies have uncovered proteins that are directly involved in crystallization mechanisms, including matrix-assisted orientation of crystals [4], growth inhibition by face-selective surface adsorption [5] and control of the crystal phase [6]; these proteins were isolated from the biominerals and analyzed. On the basis of these studies, biomimetic formation of inorganic crystals has been achieved by the biomineral-associating proteins and their mimic peptides [7]. Moreover, the functional regions of organic molecules have been adopted for the development of bio-inspired materials [8] and in biomimetic nanofabrication processes [9,10].

Magnetic iron oxides such as Fe_3O_4 and γ-Fe_2O_3 are significant materials in the development of medical and diagnostic applications, such as magnetic resonance imaging [11], hyperthermia [12], cell separation [13], and drug screening [14]. For practical use of these materials in medical and diagnostic applications, the particle size and morphology are of great importance because these factors strongly affect their magnetic properties [15]. The development of reliable and reproducible methods for synthesizing uniform-sized magnetic particles has therefore been a major goal in this field over the years.

Magnetotactic bacteria produce iron oxide magnetic particles with uniform sizes and morphologies [16]. Various crystal morphologies and compositions have been observed that are species or strain dependent, indicating that there is a high degree of biological control [17,18]. In the previous study, we identified a class of proteins that tightly associated with the magnetite crystal surface in *Magnetospirillum magneticum* AMB-1 [19]. One of these proteins designated as Mms6 is amphiphilic and mainly consists of an N-terminal hydrophobic region and C-terminal hydrophilic region containing multiplets of acidic amino acids. Following competitive iron binding analysis with other inorganic cations, it has been suggested that the C-terminal region is an iron-binding site [19]. Furthermore, the protein was allowed to generate uniform magnetite crystals by *in vitro* chemical magnetite synthesis without the use of organic solvents and high temperatures [19,20]. Cuboidal magnetite crystals consisting of (1 0 0) and (1 1 1) crystal faces were formed in the presence of Mms6, whilst sharp rectangular crystals consisting of mainly (1 1 1) faces were formed in the absence of the protein

* Corresponding author. Fax: +81 42 385 7713.
E-mail address: tmatsuna@cc.tuat.ac.jp (T. Matsunaga).

0021-9797/$ - see front matter © 2009 Elsevier Inc. All rights reserved.
doi:10.1016/j.jcis.2009.11.043

[21]. Although the formation of (1 0 0) crystal faces was considered to be due to a face-specific interaction with Mms6, the functional site of the molecule has not yet been identified.

In order to characterize the role of the Mms6 protein in magnetite formation, synthetic peptides mimicking the Mms6 protein were prepared and employed for chemical magnetite synthesis. Statistical analyses of the generated crystal morphologies were conducted by transmission electron microscopy (TEM).

2. Materials and methods

2.1. Preparation of protein and peptides

The Mms6 protein was prepared as described previously [21]. Briefly, an *Escherichia coli* BL21 transformant that harbours pGEX 4T-*mms6* was cultured in Luria–Bertani broth. The cells were collected and disrupted by sonication in denaturing buffer (6 M guanidine hydrochloride, 10 mM Tris, pH 10). The supernatant was subjected to size exclusion chromatography using a fast protein liquid chromatography (FPLC) system (ÄKTAexplorer 10S, GE Healthcare Biosciences, Piscataway, NJ) with a superdex 75 10/300 GL column (GE Healthcare Biosciences, Piscataway, NJ). The purified protein was diluted in the same volume of refolding buffer (50 mM Tris–HCl, 1 mM EDTA, 0.1 M L-arginine, 1 mM glutathione (reduced), 10% (v/v) glycerol, 0.8 mM glutathione (oxidized), pH 8.0) and re-natured by dialysis in phosphate buffered saline (PBS) (pH 7.4). The GST-Mms6 was digested with thrombin (Novagen, San Diego, CA) and then applied to the FPLC system to purify Mms6.

The synthetic polypeptides were purchased from BEX (Tokyo, Japan). In this study, we focused especially on the C-terminal acidic region and N-terminal hydrophobic GL region. M6A contains the C-terminal acidic region of Mms6. GLM6A was designed such that it contained both C-terminal acidic and N-terminal hydrophobic regions. M6B and GLM6B were designed by replacing the acidic amino acids of M6A and GLM6A with lysine residues. The sequences are listed in Table 1.

2.2. Magnetite synthesis

Magnetite synthesis was performed in a glass vial by the partial oxidation method [22,23]. The reaction solution (1 ml) containing 30 mM $FeSO_4 \cdot 7H_2O$, 100 mM KOH, and 400 mM KNO_3 was prepared with either Mms6 protein or the peptides (50 μg/ml). The mixture was incubated at room temperature for 5 min with continuous bubbling of argon gas. The vial was then heated to 90 °C in a water bath for 5 min under nitrogen and incubated for another 4 h at 90 °C. During incubation, the tubes were agitated manually at 30 min intervals to ensure uniform dispersion. Products were collected magnetically using a neodymium boron magnet and washed with ultra-pure water three times.

Table 1
Amino acid sequences of peptides mimicking partial sequence of Mms6.

Protein or peptide	Amino acid sequence	Molecular weight (kDa)	Isoelectric point (pI)
Mms6	GSVVGGTIWTGKGLGLGLGLGLGA WGPIILGVVGAGAVYAYMKSRDIES AQSDEEVELRDALA	6.3	4.4
M6A	DIESAQSDEEVE	1.4	3.6
GLM6A	GLGLGLGLGLDIESAQSDEEVE	2.3	3.6
M6B	KIKSAQSKKKVK	1.4	10.7
GLM6B	GLGLGLGLGLKIKSAQSKKKVK	2.3	10.7

2.3. Characterization of magnetite crystals by TEM

The synthesized magnetic precipitates were analyzed by transmission electron microscopy (TEM). Low magnification TEM analysis was performed using a conventional TEM (H-700H, Hitachi, Japan) at 150 kV. High resolution TEM (HRTEM) analysis was performed by field emission TEM (HF2000, Hitachi, Japan) at 200 kV. Selected area electron diffraction (SAED) patterns were obtained at various camera lengths. The crystals were observed along the [1 1 0] axial zone (determined by the SAED pattern). The projection from the [1 1 0] axial zone discriminates between octahedral and cubo-octahedral shaped crystals. The precipitates were identified by indexing the diffraction patterns.

TEM photographs were digitalized and the sizes of the magnetic crystals were determined by measuring the length and width of at least 100 crystals in each sample. A particle size distribution analysis software, Mac-View (MOUNTECH Co., Ltd., Tokyo, Japan), was used to determine the sizes and circularity of the particles. The particle size was defined as the average value of the length and width of the crystal.

2.4. Localization analysis of the M6A peptide on the synthesized magnetite crystals

Magnetite particles synthesized in the presence of the biotinylated M6A peptide were prepared and used for localization analysis. The synthesized particles were reacted with fluorescence-labelled streptavidin in PBS containing 0.1% Tween 20 for 45 min. The particles were then washed with ultra-pure water three times and evaluated under a fluorescent microscope. Fluorescence images were obtained at ISO 1600 and at an exposure time of 1/15 s. Particles synthesized in the presence of the M6A peptide were analysed and those synthesized in the absence of the peptide were used as a negative control.

3. Results

3.1. TEM analysis of magnetite particles synthesized in the presence of Mms6 peptides

Magnetite particles that synthesized without the use of proteins or peptides by this method were observed under TEM; they were square or diamond-shaped with well-defined crystal faces and sharp corners (Fig. 1f). The particles were determined to have octahedral morphologies by HRTEM and SAED analyses and mainly consisted of (1 1 1) crystal faces (Fig. 1h), as described in previous work [21]. In contrast, cuboidal-shaped particles with magnetite (1 1 1) and (1 0 0) crystal faces (Fig. 1g) were formed in the presence of Mms6 (Fig. 1a). The truncated crystals were similar to those of bacterial magnetites from *M. magneticum* AMB-1 [21]. In this study, we prepared several synthetic peptides from the unique amino acid sequences of Mms6 in order to determine its functional amino acid region for the magnetite synthesis. The putative iron-binding site in the C-terminal acidic region of Mms6 comprising 12 amino acids was termed as M6A. M6B was prepared by replacing the acidic amino acids (aspartate and glutamate) of M6A with lysine. GLM6A was synthesized by attaching the N-terminal glycine and leucine repetitive sequence in Mms6–M6A. Similarly, GLM6B was designed by replacing the acidic amino acids in GLM6A with lysine. The magnetite particles synthesized in the presence of the M6A and GLM6A peptides were spherical in shape (Fig. 1b and c), similar to those formed in the presence of Mms6. In contrast, octahedral particles with sharp corners were formed in the presence of GLM6B and M6B (Fig. 1d and e). Magnetite syntheses with sodium dodecyl sulphate (SDS) were also conducted as a

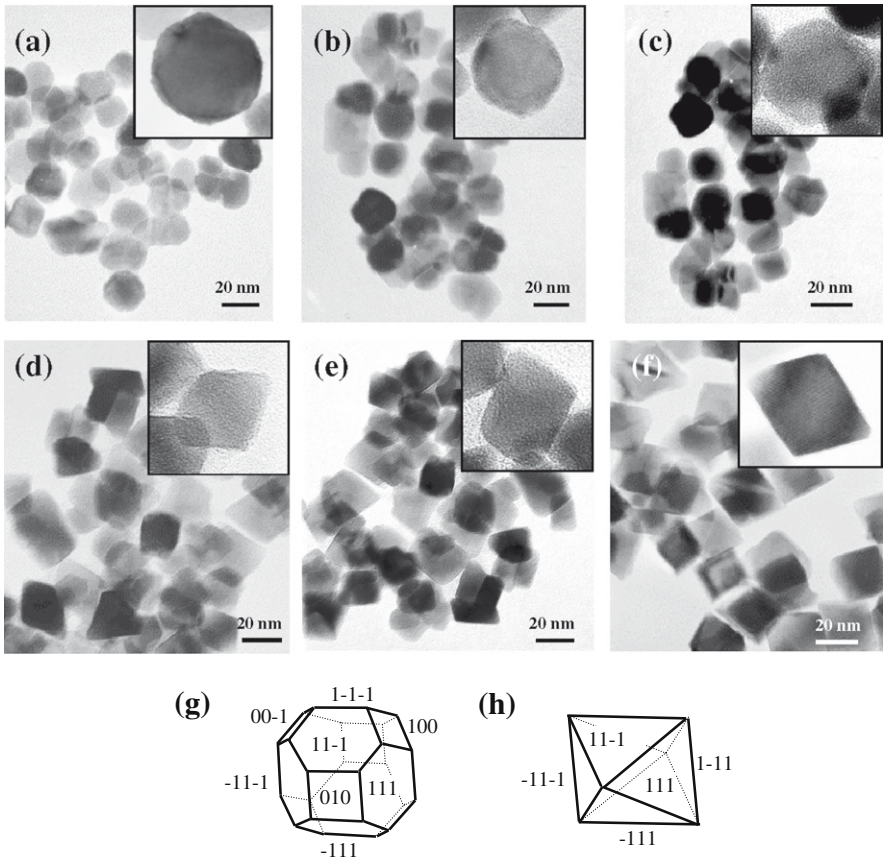

Fig. 1. TEM photographs of magnetite particles synthesized in the presence of Mms6 (a), GLM6A (b), M6A (c), GLM6B (d) and M6B (e). Particles synthesized in the absence of proteins or peptides (f). Ideal crystal morphologies: cubo-octahedron (g) and octahedron (h).

control for typical amphiphilic organic compounds. The particles formed also exhibited octahedral morphologies, similar to those of the particles formed in the absence of the peptides (Fig. S1). These results suggested that the acidic region of the Mms6 protein plays a key role in the formation of cubo-octahedral particles in the chemical synthetic reaction.

3.2. Circularity measurements of magnetite particles

In our previous study, morphological characteristics of chemically synthesized magnetic particles were individually analyzed by HRTEM and SAED [21]. However, this method is time consuming and not suitable for statistical analysis in the case of a large number of particles. In order to statistically evaluate the morphological differences in the particles prepared under different conditions, circularities of individual particles were analyzed in the TEM images. Circularity measurements were conducted by evaluating more than 100 particles in TEM images of each sample. The length and area of particles were measured and applied to the formula $[4\pi \times (\text{area})/(\text{circumference})^2]$. Therefore, the circularity of a perfect circle from a two-dimensional projection of a particle was represented as 1.00. Similarly, ideal values for a regular cubo-octahedral and octahedral shapes were designated as approximately 0.83 and 0.64, respectively. In fact, the bacterial magnetite from the AMB-1 strain, which was determined to have a cubo-octahedral crystal morphology [21], was distributed over a narrow range 0.80–0.90 with a maximum frequency of approximately 0.85 (Fig. S1c). A narrow size distribution in the range 0.70–0.90 was observed in the case of particles synthesized in the presence of Mms6 (Fig. 2a). Circularities obtained in the case of particles synthesized in the presence of GLM6A and M6A were distributed within similar ranges (Fig. 2b and c). These results suggested that a majority of the particles synthesized in the presence of Mms6, GLM6A and M6A mainly exhibit cubo-octahedral morphologies, indicating that the synthetic peptides reproduced the Mms6 function successfully. In contrast, particles synthesized in the absence of protein or peptide exhibited a wider distribution profile in the range 0.60–0.85, with a maximum frequency of approximately 0.75 (Fig. 2f). Similar profiles were obtained when particles were synthesized in the presence of GLM6B (Fig. 2d), M6B (Fig. 2e) and SDS (Fig. S1d). Although the obtained values were not in good agreement with ideal octahedron circularity, the results reveal that the characteristics of the synthetic magnetite crystals can be distinguished by this method, and it is useful for statistical analysis of morphology.

3.3. Size distribution analysis of magnetite particles

Particle size was determined by calculating the average length and width of the crystals. More than 100 particles were randomly selected and analyzed from the TEM images. Histograms of the size distribution of the synthesized magnetic particles are shown in Fig. 3. From the size distribution profiles, particles can also be classified into two groups. The particles synthesized in the absence of peptides or proteins by the partial oxidation of ferrous revealed a broad size distribution profile in the range 10–40 nm (Fig. 3f). The maximum frequency was approximately 27.5 nm. Similarly, broad distribution profiles with maxima at 25 nm were obtained in the case of particles synthesized in the presence of GLM6B (Fig. 3d), M6B (Fig. 3e) and SDS (Fig. S1f). In contrast, the distribution of particles synthesized in the presence of Mms6 (Fig. 3a) or the GLM6A peptide (Fig. 3b) were distributed in the size range 10–30 nm with maxima at 20 nm. Slightly larger maximum fre-

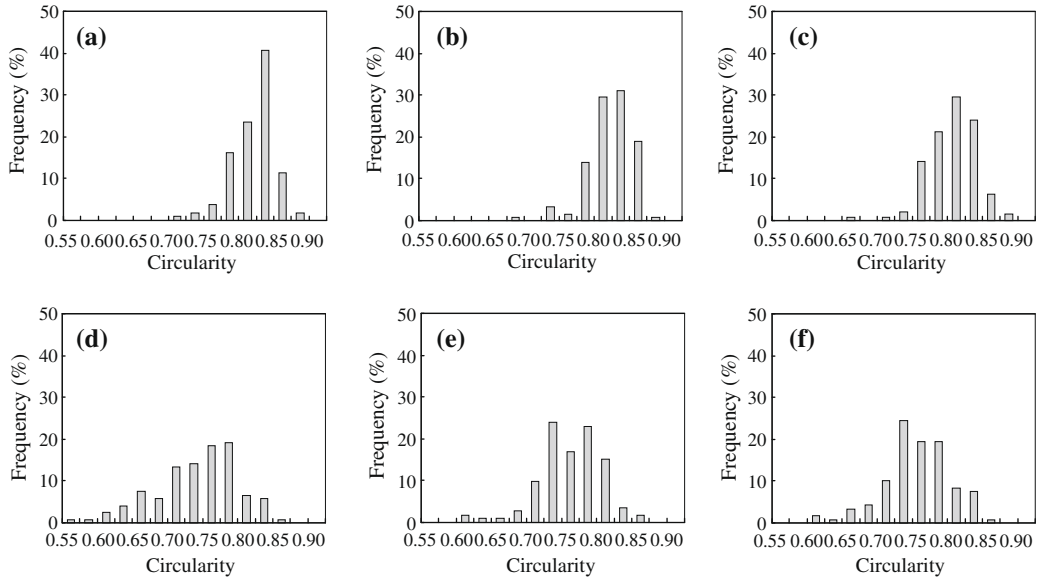

Fig. 2. Circularity distribution profiles of synthesized magnetic particles in the presence of Mms6 (a), GLM6A (b), M6A (c), GLM6B (d) and M6B (e). Distribution profile of particles synthesized in the absence of proteins and peptides (f).

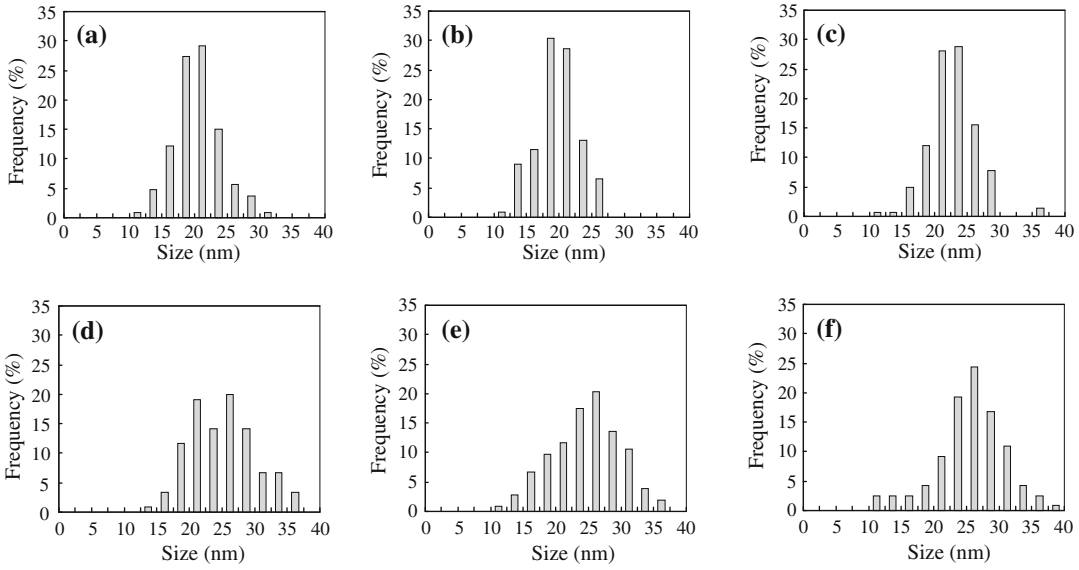

Fig. 3. Size distribution profiles of synthesized magnetic particles in the presence of Mms6 (a), GLM6A (b), M6A (c), GLM6B (d) and M6B (e). Distribution profile of particles synthesized in the absence of proteins or peptides (f).

quencies, i.e. approximately 20–25 nm, were observed in the case of M6A (Fig. 3c), which may be due to the lack of the repetitive glycine and leucine sequence in GLM6A. Moreover, the distributions of the particles formed in the presence of Mms6, GLM6A and M6A were narrower and smaller than those formed in the presence of GLM6B, M6B and SDS. The observed size reduction was due to the morphological changes in the crystals from octahedral to cubo-octahedral.

3.4. Localization analysis of the M6A peptide

Localization of peptides on the synthesized magnetite particles was investigated by the fluorescence labeling technique. C-terminal biotinylated M6A peptides were utilized for magnetite synthesis. After the synthesis, unbound biotinylated peptides were removed from the reaction mixture, and Cy5-labeled streptavidin was added to the solution. Magnetite particles synthesized in the presence of the biotin labeled-M6A peptide exhibited a bright fluorescence under the fluorescent microscope (Fig. 4a). In contrast, no significant fluorescence was observed in the case of particles synthesized in the presence of the non-biotinylated M6A peptide (Fig. 4b) or in the absence of the peptide (Fig. 4c). This result indicates that the M6A peptides are located on the surface of synthesized magnetite particles.

4. Discussion

In this study, magnetite synthesis was examined in the presence of short peptides mimicking the Mms6 protein by the partial oxidation method. The reaction scheme was as follows [22,24]:

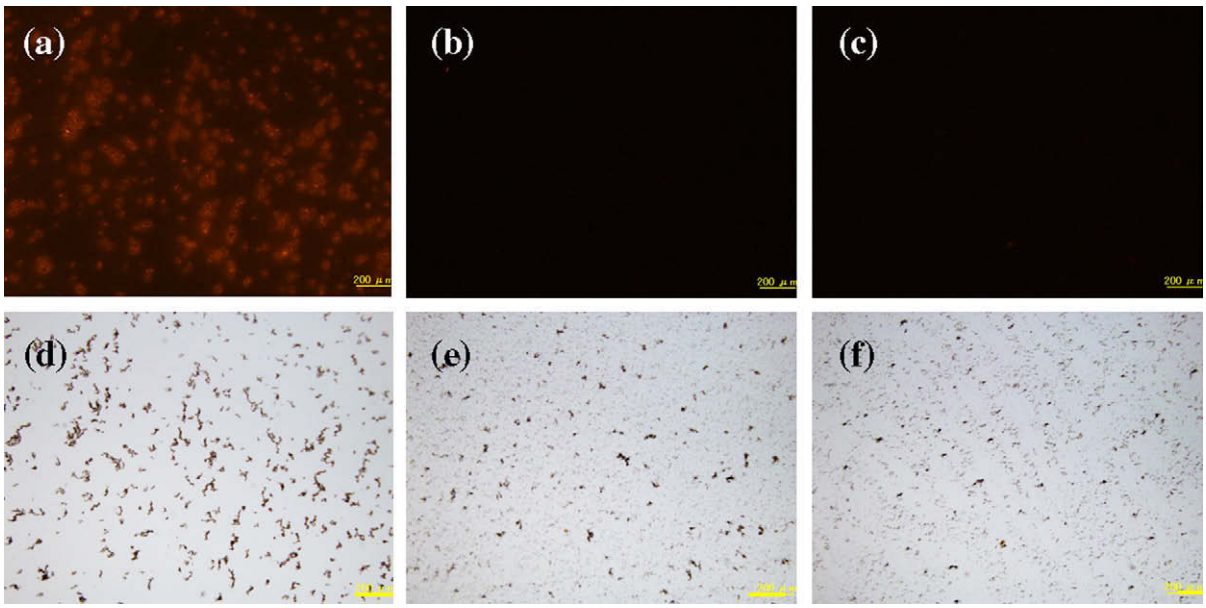

Fig. 4. Localization of the M6A peptide on the synthesized magnetic particles. Fluorescence (a–c) and light (d–f) microscopic photographs of magnetite particles synthesized in the presence of biotin-M6A (a, d) and M6A (b, e). Particles synthesized in the absence of peptides (c, f). The particles were reacted with tetramethylrhodamine-labelled streptavidin after the synthesis. Scale bars = 200 μm.

$$2Fe^{2+} + 4OH^- \rightarrow 2Fe(OH)_2 \quad (1)$$

$$2Fe(OH)_2 + NO_3^- + H_2O \rightarrow 2Fe(OH)_3 + NO_2^- \quad (2)$$

$$Fe(OH)_2 + 2Fe(OH)_3 \rightarrow Fe_3O_4 + 4H_2O \quad (3)$$

In our investigation, a ferrous solution containing either protein or peptide was maintained under anoxic conditions at room temperature. During the reaction (reaction scheme Eqs. (1) and (2)), the color of the ferrous solution changed from transparent blue to bluish green. The observed non-magnetic green precipitate is considered to be mainly composed of iron hydroxide ($Fe(OH)_2$ and $Fe(OH)_3$) [22]. The co-existence of Mms6 polypeptides in the iron solution seems to either accelerate or stabilize the iron hydroxide-formation process [21]. Magnetite formation was then evident due to the progressive conversion of the initially non-magnetic green precipitate into a strongly black magnetic precipitate when the solution was heated to 90 °C (reaction scheme (3)). The reaction at room temperature yields primary small iron hydroxides that aggregate to form a larger iron hydroxide core [22]. Mms6 and the mimic peptides in the iron solution are considered to be involved in the acceleration or stabilization of the iron hydroxide-formation process.

The magnetite (1 1 1) and (1 0 0) surfaces are stable, and they are the most distinct crystal faces in natural magnetites [24]. The magnetite (1 1 1) surface possesses complicated atomic structures and is proposed to form 6 possible terminations [25], while the (1 0 0) plane is proposed to form a stacking sequence of 2 alternating layers [26]. These surface structures are also known to be highly sensitive to the surrounding atmosphere. Although the atomic structures of these surfaces in water are poorly understood, they form distinct characteristic surfaces that associate with Fe^{2+}, Fe^{3+} and oxygen ions. In fact, it was revealed that the surface structures of magnetite (1 0 0) and (1 1 1) influence the cell adhesion of dissimilatory iron-reducing bacteria [27]. The differences in the adhesive forces observed between (1 0 0) and (1 1 1) were explained by the electrostatic and hydrophobic interactions of the cells and the mineral surface. The formation of the cubo-octahedral morphology with (1 0 0) crystal faces in the presence of Mms6 and the mimic peptides is probably relevant to the coordination interaction between the inorganic surfaces and the polypeptides.

Interactions between the organic molecules and inorganic crystal surfaces play a central role in biomineralization [28,29]. However, there are only a few reports that have elucidated direct interactions between the protein and specific crystal surface [5,30]. A protein abundant in urine, osteopontin, induces the formation of dumbbell-shaped calcium oxalate monohydrate crystals with well-developed (0 2 1) faces and round edges [5]. The protein was preferentially adsorbed on the edges between the (1 0 0) and (1 2 1) faces of the calcium oxalate monohydrate crystals. This edge-specific binding of osteopontin was proposed to be responsible for both the development of (0 2 1) crystal faces and the dumbbell morphology. We have also revealed direct binding of the M6A peptide to the formed magnetite crystals by fluorescent microscopy. This observation is consistent with the result of a protein assay in the previous report [21]. Alternatively, the mechanism of magnetite (1 0 0) crystal face formation might be similar to that of the edge-specific interaction of polypeptides. Specific localization of proteins or peptides onto particular crystal faces or edges could not determined in this study, but this will be clarified by further investigations, such as TEM immunogold staining [31].

In the *in vitro* mineral synthesis, the morphology of the minerals can be attributed to the conformation and self-organization of polypeptides. The goose-eggshell-matrix protein, ansocalcin, was found to induce the formation of polycrystalline aggregates of calcite crystals in *in vitro* mineralization experiments [32]. In addition, mimicking the protein function was successfully achieved by using synthetic peptides and including the specific amino acid sequence of ansocalcin [7]. The effect of the ordered arrangement of charged residues and self-assembling characteristics of the synthetic peptides on the calcite crystal morphology was also revealed. Although the exact role of the hydrophobic region of Mms6 still remains unknown, self-aggregation at the N-terminal hydrophobic region was observed in solution [21]. The circular dichroism (CD) spectrum of this protein revealed the presence of a random coil structure with an α-helical conformation which is most probably derived from the C-terminal acidic region. Moreover, the results of this study indicated that the negatively charged C-terminal region is crucial for the formation of cubo-octahedral crystals. However, the observed size and morphology of the

crystals synthesized in the presence of Mms6 and other mimic peptides cannot be attributed to only the isoelectric points or the net negative charge of these molecules because magnetite synthesis in the presence of BSA (pI, 4.7) did not significantly affect crystal characteristics [21]. The conformation of the C-terminal region, consisting of a number of negatively charged amino acids, may contribute to controlling the morphology of the magnetite crystals.

5. Conclusions

In this study, we designed short synthetic peptides that mimicked the functions of the characteristic amino acid sequences of Mms6, and utilized them for *in vitro* chemical magnetite synthesis. Magnetite synthesis using peptides containing the C-terminal acidic region of Mms6 resulted in the formation of uniform-sized cubo-octahedral crystals with a narrow size distribution. The morphological characteristics were confirmed by statistical evaluation of the size distribution and circularity from TEM images. These results indicated that the magnetite particles synthesized by the chemical synthetic method with the Mms6 peptides exhibited similar crystal characteristics as those of biogenic magnetite, and this method presents an alternative route for controlling the size and shape of magnetite crystals without the use of organic solvents and high temperatures.

Acknowledgments

This work was funded by the Industrial Technology Research Grant Program in 2006 from the New Energy and Industrial Technology Development Organization (NEDO) of Japan.

Appendix A. Supplementary material

Supplementary data associated with this article can be found, in the online version, at doi:10.1016/j.jcis.2009.11.043.

References

[1] C. Du, G. Falini, S. Fermani, C. Abbott, J. Moradian-Oldak, Science 307 (2005) 1450.
[2] M. Sumper, E. Brunner, Chembiochem 9 (2008) 1187.
[3] A. Perez-Huerta, M. Cusack, W. Zhu, J. England, J. Hughes, J. R. Soc. Interface 4 (2007) 33.
[4] S. Gajjeraman, K. Narayanan, J. Hao, C. Qin, A. George, J. Biol. Chem. 282 (2007) 1193.
[5] A. Taller, B. Grohe, K.A. Rogers, H.A. Goldberg, G.K. Hunter, Biophys. J. 93 (2007) 1768.
[6] L.F. Huitema, P.R. van Weeren, B.W. van Balkom, T. Visser, C.H. van de Lest, A. Barneveld, J.B. Helms, A.B. Vaandrager, Biochim. Biophys. Acta 1774 (2007) 1108.
[7] P. Ajikumar, S. Vivekanandan, R. Lakshminarayanan, S. Jois, R. Kini, S. Valiyaveettil, Angew. Chem. Int. Ed. 44 (2005) 5476.
[8] H. Bai, K. Xu, Y. Xu, H. Matsui, Angew. Chem. Int. Ed. 46 (2007) 3319.
[9] J. Aizenberg, D.A. Muller, J.L. Grazul, D.R. Hamann, Science 299 (2003) 1205.
[10] D. Kisailus, Q. Truong, Y. Amemiya, J.C. Weaver, D.E. Morse, Proc. Natl. Acad. Sci. USA 103 (2006) 5652.
[11] C. Sun, O. Veiseh, J. Gunn, C. Fang, S. Hansen, D. Lee, R. Sze, R.G. Ellenbogen, J. Olson, M. Zhang, Small 4 (2008) 372.
[12] A. Ito, H. Honda, T. Kobayashi, Cancer Immunol. Immunother. 55 (2006) 320.
[13] T. Matsunaga, M. Takahashi, T. Yoshino, M. Kuhara, H. Takeyama, Biochem. Biophys. Res. Commun. 350 (2006) 1019.
[14] T. Yoshino, M. Takahashi, H. Takeyama, Y. Okamura, F. Kato, T. Matsunaga, Appl. Environ. Microbiol. 70 (2004) 2880.
[15] V.F. Puntes, K.M. Krishnan, A.P. Alivisatos, Science 291 (2001) 2115.
[16] T. Matsunaga, T. Suzuki, M. Tanaka, A. Arakaki, Trends Biotechnol. 25 (2007) 182.
[17] F.C. Meldrum, S. Mann, B.R. Heywood, R.B. Frankel, D.A. Bazylinski, Proc. R. Soc. Lond. B 251 (1993) 231.
[18] F.C. Meldrum, S. Mann, B.R. Heywood, R.B. Frankel, D.A. Bazylinski, Proc. R. Soc. Lond. B 251 (1993) 237.
[19] A. Arakaki, J. Webb, T. Matsunaga, J. Biol. Chem. 278 (2003) 8745.
[20] T. Prozorov, S.K. Mallapragada, B. Narasimhan, L.J. Wang, P. Palo, M. Nilsen-Hamilton, T.J. Williams, D.A. Bazylinski, R. Prozorov, P.C. Canfield, Adv. Funct. Mater. 17 (2007) 951.
[21] Y. Amemiya, A. Arakaki, S.S. Staniland, T. Tanaka, T. Matsunaga, Biomaterials 28 (2007) 5381.
[22] T. Sugimoto, E. Matijevic, J. Colloid Interface Sci. 74 (1980) 227.
[23] B. Devouard, M. Pósfai, X. Hua, D.A. Bazylinski, R.B. Frankel, P.R. Buseck, Am. Mineral. 83 (1998) 1387.
[24] R.M. Cornell, U.S. Schwertman, The Iron Oxides, Wiley-VCH, Weinheim, 2003.
[25] A.R. Lennie, N.G. Condon, F.M. Leibsle, P.W. Murray, G. Thornton, D.J. Vaughan, Phys. Rev. B 53 (1996) 10244.
[26] S.F. Ceballos, G. Mariotto, K. Jordan, S. Murphy, C. Seoighe, I.V. Shvets, Surf. Sci. 548 (2004) 106.
[27] A.L. Neal, T.L. Bank, M.F. Hochella, K.M. Rosso, Geochem. Trans. 6 (2005) 77.
[28] V. Gerbaud, D. Pignol, E. Loret, J.A. Bertrand, Y. Berland, J.C. Fontecilla-Camps, J.P. Canselier, N. Gabas, J.M. Verdier, J. Biol. Chem. 275 (2000) 1057.
[29] M. Michenfelder, G. Fu, C. Lawrence, J.C. Weaver, B.A. Wustman, L. Taranto, J.S. Evans, D.E. Morse, Biopolymers 70 (2003) 522.
[30] B. Grohe, J. O'Young, D.A. Ionescu, G. Lajoie, K.A. Rogers, M. Karttunen, H.A. Goldberg, G.K. Hunter, J. Am. Chem. Soc. 129 (2007) 14946.
[31] T. Yoshino, T. Matsunaga, Appl. Environ. Microbiol. 72 (2006) 465.
[32] R. Lakshminarayanan, R. Kini, S. Valiyaveettil, Proc. Natl. Acad. Sci. USA 99 (2002) 5155.